2023 IEEE/ASME International Conference on Advanced Intelligent Mechatronics (AIM)
June 28-30, 2023. Seattle, Washington, USA

Haptic Interface Design for a Novel Wheelchair Simulator using Linear Time-Varying MPC Framework

A. Ait-Ghezala, C. Sentouh, , T. Bentaleb, P. Pudlo, T. Poulain, G. Conreur

***Abstract*—This paper deals with the design of a new haptic interface to drive a wheelchair locomotion simulator in real-time. The proposed haptic interface considers a reference model of a manual wheelchair (MWC) with a coupled straight line, turn and slope/cross-slope dynamics. This model allows both to reproduce the wheel-ground contact resistances in real-time and to estimate the kinematic motion states of the wheelchair. Then the theoretical concept of the model predictive control (MPC) scheme for linear time-varying (LTV) systems is exploited for the design of the haptic controller in order to handle the reference tracking problem. This controller is based on an LTV model of the MWC system coupled with the ergometer rollers of the simulator using an online identification of its dynamics. This formulation allows us to deal with nonlinearities and variations of the contact friction between the MWC wheels and the simulator rollers. The stability of the simulator haptic interface is demonstrated using the Lyapunov stability tools. Finally, the performance and effectiveness of the proposed haptic interface are evaluated by experimental tests on the PSCHITT-PMR simulator platform using standardized locomotion scenarios.**

***Index Terms*—Wheelchair Simulator, haptic interface, real-time applications, model predictive control (MPC), linear time-varying (LTV) systems, people with motor disabilities.**

I. Introduction

The manual wheelchair (MWC) is an essential tool for the empowerment of people with reduced mobility. Thus, better accessibility for wheelchair users promotes, a balanced and better quality of life. However, wheelchair accessibility is still not assured for many manual wheelchair users, due to inadequate urban infrastructure but also the physical capabilities of the user [1]. Therefore, it is crucial to thoroughly investigate the biomechanical efficiency of the MWC propulsion as a function of the driving environmental conditions. In general, to quantify the energy losses during wheelchair movement, it is sufficient to evaluate the rolling and pivoting resistance torques [2]. One of the main limits of this approach is that it is based on a long and costly experimental process, and that can be dangerous for the subjects. A more promising solution for an experimental laboratory setup is a wheelchair locomotion simulator [3]–[6]. It simulates the locomotion of a manual (MWC), electric, and power-assisted wheelchair in a virtual environment for various driving situations. In this way, realistic accessibility conditions are created, opening up many solutions to enable ergonomic wheelchair locomotion with the aim of providing a reliable examination of the biomechanics of wheelchair propulsion. Nevertheless, the design of haptic interfaces to drive such systems is quite complex. Among the current simulators, there are treadmills that can replicate the straight-line movements of the MWC on flat or sloping ground [3], [7], although the wheels of the wheelchair are constrained to the same speed and direction, which limits this type of simulator to reproduce the propulsion during turning or slope maneuvers. Another common simulator is the dyno-ergometer [8]–[10]. It allows a combination of straight and turning movements on flat ground. However, the main scientific limitation of these simulators is the ability to reproduce in real-time the resistances applied to the wheels of the real ground in the virtual environment for a combination of a straight line, turn, or maneuvers on the ground with slope/cross-slope depending on the user's actions. In fact, such systems require haptic interfaces that can drive the simulator to realistically reproduce wheelchair displacement in the virtual environment (VE). Several haptic interfaces for MWC simulators are proposed in the literature, usually based on a simple MWC model and a basic controller to simulate friction between the wheels and the ground [6]. In [8] a haptic interface prototype was developed to generate an interaction between a virtual environment and the dynamics of the wheels allowing the movement of the MWC in the VE, however, the resistances applied on the wheels are not considered. In [11], a more interesting simulator is proposed. It combines both VE immersion and haptic force feedback. However, this haptic controller is based on a model with constant contact friction, even though, its dynamics has a significant influence on the behavior of the MWC dynamics. In [12] an MWC simulator composed of a hexapod to simulate tilting movements was proposed. However, there is no mention of wheel-ground contact dynamics. The challenge of designing systems combining immersion and haptic feedback is discussed in the paragraph. Haptic feedback simulators are limited by simplistic dynamic models and do not consider several physical parameters, which reduces their realism. On the other hand, interactive platforms, such as virtual reality simulators, offer better immersion, but have fewer haptic feedback features. Finally, most of the current simulators have limited movements, highlighting the need for more advanced solutions. In this paper, A new haptic and immersive simulator named PSCHITT-PMR has been developed to provide a personalized experience for users. The simulator includes a hexapod with six degrees of freedom, six integrated displays, an ergometer equipped with haptic rollers and an instrumented wheelchair, all controlled remotely by a computer. Biomechanical quantities are measured by the

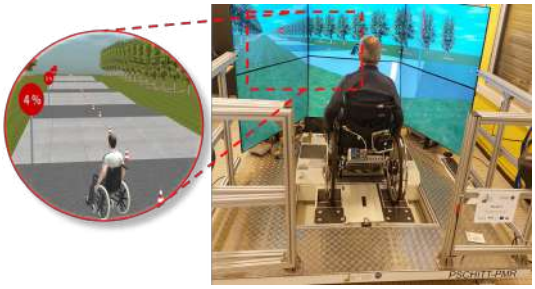

Fig. 1. Image of PSCHITT-PMR Simulator

instrumented wheelchair, and haptic feedback is provided to account for the contact forces between the wheelchair and the ground. The SCANeR Studio software environment ensures the immersive aspect of the simulator, Fig. 2. The design of a custom haptic interface to drive a wheelchair locomotion simulator in a realistic virtual environment is presented. The interface considers a full MWC model with coupled straight line, curved and slope/across dynamics, allowing to reproduce wheel-ground contact resistances in real time and to estimate the kinematic motion states of the wheelchair. A haptic controller based on a linear time-varying (LTV) model of the simulator dynamics is built to handle the non-linearities of the contact friction between the MWC wheels and the simulator rollers and to adapt to the user's characteristics. The MPC optimal control algorithm for LTV systems [20], [21] is exploited to design the haptic controller, using Lyapunov's stability proof to ensure optimal simulator performance. The controller generates haptic feedback felt by the user during the push phase and vertical inertial translation of the wheelchair during the release phase, thus providing a realistic wheelchair locomotion experience. To assess the effectiveness of the haptic interface, various standardized locomotion scenarios that are typically encountered in an urban setting are defined and implemented in the PSCHITT-PMR wheelchair simulator. The remainder of the paper is organized as follows. The remainder of the paper outline of the paper's structure. Section II will provide an overview of the haptic interface of the PSCHITT-PMR wheelchair simulator. In Section III, the design of the haptic controller will be presented. Section IV will cover the experimental procedure, results, and discussion. Finally, in Section V, the conclusions of the paper will be drawn.

II. Model Reference-based Haptic Interface

The PSCHITTPMR simulator was developed in the LAMIH laboratory, specifically designed for research in the field of assistance for people with reduced mobility. In this particular configuration, PSCHITTPMR offers a realistic virtual environment, guaranteeing a global vision and allowing the movement of a wheelchair in all locomotion situations.

A. User-Wheelchair-Environment Modeling

The MWC dynamics generated by the simulator must produce the same sensory-motor state as when the wheelchair is propelled on real ground. Thus, the reliability of the simulator relies on the realism provided by the mechanical model of MWC-user interactions. Unlike models used in current ergometers, the MWC model considered in this work provides in real-time, the complete dynamics of the wheelchair locomotion in straight line, turn and slope/cross-slope while considering the rolling and pivoting resistive torques.

1) General Manual Wheelchair Motion Model: The considered MWC model has 7-degree-of-freedom (DOF). Mainly used to describe vehicle dynamics, this model has been adapted to the wheelchair dynamics considering straight line X, lateral Y and yaw ψ motions with the slope/cross-slope environment inputs [15]–[17]. We assume that the dynamics of vertical, pitch, and roll are neglected. Thus, the MWC dynamics is expressed as follows

- Longitudinal, lateral and yaw motions dynamics

$$\begin{aligned} m\dot{v}_x &= \sum_{i=3,4} F_{x_i} + \sum_{i=1,2} F_{xp_i} + F_{x_G r} - F_{rr} + m v_y \dot{\psi} \\ m\dot{v}_y &= \sum_{i=3,4} F_{y_i} + \sum_{i=1,2} F_{yp_i} + F_{y_G r} - m v_x \dot{\psi} \\ J_z \ddot{\psi} &= d_f F_{yci} cos(\phi) - d_f F_{xci} sin(\phi) - d_r F_{y_r i} \\ &\quad + T_{res} - T_{fr} \end{aligned} \tag{1}$$

- Wheels rotational movements

$$\begin{aligned} J_{r_i} \dot{\omega}_{r_i} &= T_{h_i} - R_{r_i} F_{x_i} - \eta \omega_{r_i} + T_{rr_i}, \quad i \in \{3,4\} \\ J_{f_i} \dot{\omega}_{f_i} &= -R_{f_i} F_{x_i} - \eta \omega_{f_i} + T_{rr_i}, \quad i \in \{1,2\} \\ J_{c_i} \ddot{\varphi}_{c_i} &= d_{ci}(F_{yci} + F_{xci}) \quad i \in \{1..2\} \end{aligned} \tag{2}$$

Equation (1) represents the dynamics of the longitudinal, lateral and yaw motions at the center of gravity. Equation (2) describes the rotational wheel motions including the acceleration and braking motions of the front and rear wheels, $\omega_{(f,r)}$, as well as the yaw rotational motion of the front free castors φ_{c_i}. Terms M, J_z, and J_{c_i} are respectively the mass of the wheelchair, the inertia around the z-axis at the center of gravity, and the inertia around the z-axis at the front wheel pivot. While J_{r_i} and J_{f_i} are the inertia of the rear and front wheels.

2) Wheel-Ground Contact Force Dynamics: The accuracy of the contact force models is crucial to reproduce the resistances applied to the wheels during the movement in the virtual environment. Generally, a linear model is used to describe torque resistances. However, in various locomotion situations, such as the starting movement or combined maneuvers, the linear model becomes invalid. For this reason, the Pacejka tire model [16], called "the Magic Formula", is used in this work. This tire model is one of the most widely used in the literature to accurately describe the behavior of the nonlinear slip force and resistance torque in vehicle dynamics. The MWC tire-road contact in the longitudinal direction is modeled by the following equation

$$\begin{aligned} F_{x_i} = D_i sin(C_i \ atan(B_i \mu_i - E_i(B_i \mu_i \\ - \ atan(B_i \mu_i)))) \ F_{z_i} \end{aligned} \tag{3}$$

TABLE I
PHYSICAL VARIABLES DESCRIPTION

Physical Variables	Description
F_{x_i}, F_{x_i}	Longitudinal and lateral forces [N]
T_{h_i}, $T_r r$	Human torque and rolling resistance torque $[Nm]$
ω_{r_i}, ω_{f_i}	Angular speeds of the rear and front wheels $[rads^{-1}]$
v_x, v_y	Longitudinal and lateral speeds$[ms^{-1}]$
$\dot{\psi}$, T_{res}	Yaw rate $[rads^{-1}]$ and yaw resistance torque $[Nm]$
$F_{xg}r$, $F_{yg}r$	Gravity forces according to x and y positions $[N]$

TABLE II
WHEELCHAIR MODEL PARAMETERS

Parameters	Value [Unit]	Parameters	Value [Unit]
M	100 $[kg]$	η	0.05 $[kgm^2s^-1]$
J_z	7 $[kgm^2]$	J_{ci}	0.05 $[kgm^2]$
$J_{\omega_{ri}}$	1.5 $[kgm^2]$	$J_{\omega_{fi}}$	0.1 $[kgm^2]$
w_r	0.60 [m]	w_f	0.48 [m]
d_r	0.22 [m]	d_r	0.22 [m]
R_{f_i}	0.31 [m]	R_{r_i}	0.065 [m]
$\mu_r r$	0.01	$k_{\dot{\psi}}$	10
α	8	β	8.5
γ	9.5	λ	9
B	2	C	2
D	0.2	E	0.8
$C_{\alpha_{ri}}$	1.72 $[rad^{-1}]$	$C_{\alpha_{fi}}$	6 $[rad^{-1}]$

The terms D_i, C_i, B_i and E_i are the intrinsic characteristic parameters of the wheel's tires. μ_i is the longitudinal slip ratio.

$$\mu_r = \frac{R_{r_i}\omega_{r_i} - v_{x_i}}{max(v_{x_i}, R_{r_i}\omega_{r_i})} \quad \text{and} \quad \mu_f = \frac{R_{f_i}\omega_{f_i} - v_{x_i}}{max(v_{x_i}, R_{f_i}\omega_{f_i})} \tag{4}$$

During the lateral movement of the MWC, the dynamics involved in this direction is not significant; therefore, the lateral force F_y can be approximated using a linear model.

$$F_{y_r} = -C_{\alpha_{r_i}}\alpha_{r_i}F_{z_i} \quad \text{and} \quad F_{y_f} = -C_{\alpha_{f_i}}\alpha_{f_i}F_{z_i} \tag{5}$$

where $C_{\alpha_{r_i}}$ and $C_{\alpha_{f_i}}$ are the tire stiffness coefficients normalized with the MWC's wheel vertical force, respectively, for the rear and front MWC wheels. As shown in Fig. 2, α_{r_i} and α_{f_i} are, respectively, the lateral slip angles of the rear and front wheels. In order to create the lateral displacement resistance effect during the MWC yaw motion, a resistant torque mathematical model, T_{res}, has been developed

$$T_{res}(\dot{\psi}) = k_{\dot{\psi}}\left(1 - e^{-\alpha\dot{\psi}}\right)\left(\frac{1 + \tanh\left(\beta\dot{\psi} - \gamma\right)}{2}\right) \left(\lambda - (\lambda - 1)\tanh\left(\beta\dot{\psi} - \gamma\right)\right) \tag{6}$$

The parameters $k_{\dot{\psi}}$, α, β, γ, and λ are the resistant torque model parameters needed to be identified. This model calculates, in real-time, the resistant torque taking into account the region of zero yaw velocity to deal with the chattering problem and allowing us to avoid algebraic loops problems during the numerical simulation. The wheelchair reference model is validated using experimental data [10].

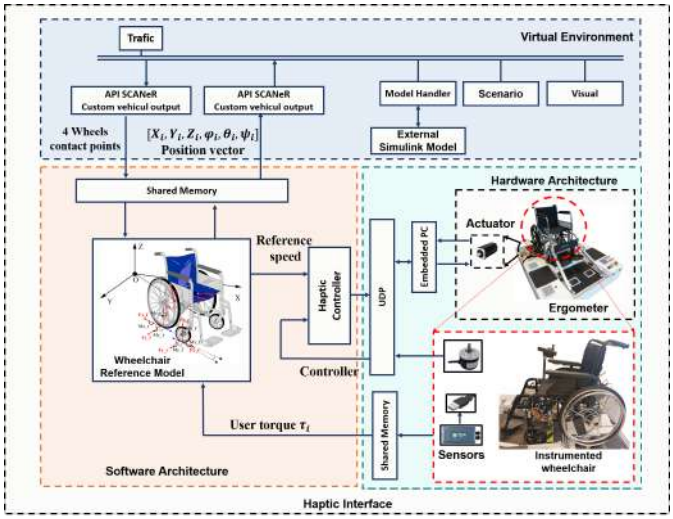

Fig. 2. Descriptive diagram of the PSCHITT-PMR simulator driven by the designed haptic interface.

III. OPTIMAL LTV-MPC-BASED HAPTIC INTERFACE CONTROL DESIGN

A. Wheelchair-Ergometer Model Estimation

As mentioned in the introduction, a nonlinear and uncertain simulator model could decrease the controller performance, as the optimization problem becomes computationally intensive. For this reason, an online identification-based LTV model can successively estimate the nonlinear contact friction between the MWC wheels and the simulator rollers. The standard expression for the contact friction behavior between wheelchair wheels and simulator rollers can be written as follows [18]

$$\begin{cases} \mathcal{I}_L\dot{\Omega}_L(t) - \mathcal{N}_L((\Theta_i, \Omega_L(t)) = K_\tau\ \tau_L(t) + \tau_{h_L}(t) \\ \mathcal{I}_R\dot{\Omega}_R(t) - \mathcal{N}_R(\Theta_i, \Omega_R(t)) = K_\tau\ \tau_R(t) + \tau_{h_R}(t) \end{cases} \tag{7}$$

Equations (7) express the wheel-roller dynamics on each left (L) and right (D) side of the simulator. Where $\dot{\Omega}$ and Ω are the angular acceleration and angular velocity of the wheel. τ_h is the propulsive human torque applied on the hand-rim. The parameter K_τ represents the reduction ratio between the wheel and the roller, whereas $\mathcal{N}_i(\Theta_i, \Omega_i(t))$ is the contact friction torque model. In the following, we assume that contact friction can be linearly parameterized as an affine relationship between $\mathcal{N}_i(t) \in \mathbb{R}_n$ and $\Omega_i \in \mathbb{R}_p$ and that there is no slipping during movement

$$\mathcal{N}_i(t) = \Theta_1(t)\ \Omega_{L,R}(t) + \Theta_2(t) \tag{8}$$

Here, $\Theta_1(t)$ and $\Theta_2(t)$ are unknown time-varying parameters. $\Theta(t) = [\Theta_1(t), \Theta_2(t)]^T$ can be determined in real-time using the measured data pairs $(\tau_{L,R}, \Omega_i), i = 1, 2, ..., N_r$. It should be noted that, in this work, the objective is to simplify the nonlinear model of the contact friction torque between the wheelchair and the simulator ergometer rollers. To estimate the unknown time-varying parameters in equation (8), an online recursive least squares identification algorithm (RLS) is considered [19]. Using an online identification algorithm not only allows us to estimate the contact friction dynamics in real-time, i.e., but also ensures a successive linearization of the nonlinear model around the current operating point at each time step without introducing a recursive algorithm into the MPC optimization scheme. In the next subsection, a linear MPC is designed for the resulting wheelchair-ergometer LTV system.

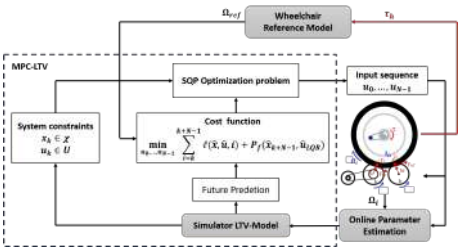

Fig. 3. Block diagram of the MPC controller of the closed loop simulator

B. LTV-MPC Controller Design

In the present part, we introduce the theoretical concepts of model predictive control for time-varying linear discrete-time systems. The stability of the closed-loop model predictive control is demonstrated based on the extensive literature [20]–[22]. Consider the time-varying linear discrete-time (LTV) systems with hard input and state constraints given by

$$\Sigma_{LTV} = \begin{cases} x(k+1) = A(k)\ x(k) + Bu(k) + d(k) \\ y(k) = Cx(k) \end{cases} \tag{9}$$

Where $x(k) \in \mathbb{R}^n$ is the state of the system, $u(k) \in \mathbb{R}^m$ is the control input in the current time sample k and $x(k+1)$ is the prediction of the state in the sample k. The control input and the state are time-varying and must satisfy the following constraints

$$\begin{aligned} x(k) \in \mathbb{X}(k) &= \{x \ : \ |x| \leq x_{max}\} \\ u(k) \in \mathbb{U}(k) &= \{u \ : \ |u| \leq u_{max}\} \\ x(N) &\in \mathbb{X}_f(k) \end{aligned} \tag{10}$$

Where $\mathbb{U}(k)$ is a compact subset $\mathbb{U}(k) \in \mathbb{R}^m$, $\mathbb{X}(k)$ is a closed convex subset $\mathbb{X}(k) \in \mathbb{R}^n$ with the origin included in each subset and $x(N) \in \mathbb{X}_f(k)$ is a terminal constraint set. In the following, we assume that there exist positive constants radius r_1 and r_2 such that $\mathbb{X}(k) \supseteq \mathcal{B}_{r_1}$, $\mathbb{U}(k) \supseteq \mathcal{B}_{r_2}\ \forall\ k \geq t$ with $\mathcal{B}_r = \{x \in \mathbb{R}^n : \|x\| \leq r\}$. The state model (9) is a first-order approximation of the non-linear model (7) over a time horizon $i = k, ...k+N-1$, where $N \in \mathbb{Z}^+$ is the predicted horizon chosen sufficiently large to cover the transient state of the system. The time-varying parameter $A(k)$ is bounded, such that $\forall\ i \geq k\ : \|A(k)\| \leq \Theta_A$ in which Θ_A is a finite positive constant. B and the vector $d(k)$ are known and the pair $(A(k),B)$ is uniformly stabilizable. Furthermore, a full-state measurement of $x(k)$ is available at sample time k. Thus, we can formulate the time-varying optimal control problem to be solved with the MPC approach as follows:

$$\begin{aligned} \mathcal{V}(\hat{x}, \hat{U}, k)^* = \min_{U_k} \Bigg\{ & \sum_{i=k}^{k+N-1} \hat{x}^T(i) Q \hat{x}(i) + \hat{u}^T(i) R \hat{u}(i) \\ & + \hat{x}^T_{k+N-1} P_f \hat{x}_{k+N-1} \mid u \in \mathbb{U} \Bigg\} \end{aligned} \tag{11a}$$

$$\begin{aligned} & s.t. \\ & x_k(i+1) = A_k(\Theta_i) x_k(i) + B u_k(i) + d_k(i), \quad i=k,\dots,N-1 \\ & u_k(i) \in \mathbb{U}(k), \quad i=k,\dots,k+N-1 \\ & x_k(i) \in \mathbb{X}(k), \quad i=k,\dots,k+N \\ & x_k(k+N) \in \mathbb{X}_f(k) \\ & x_k(k) = x(k) \end{aligned} \tag{11b}$$

in which $\hat{x}(k) = [\hat{x}(k), \dots, \hat{x}(k+N)]$ is the error trajectory between the predicted state $x(k) = [x(k), \dots, x(k+N)]$ and the reference trajectory $\Omega_{ref}(k) = [\Omega_{ref}(k), \dots, \Omega_{ref}(k+N)]$ over the time horizon $k+N$ and $\hat{u}(k) = [\hat{u}(k), \hat{u}(k+1), \dots, \hat{u}(k+N-1)]$ is the control variable to be optimized at time k. The pair matrix (Q, R) and (Q_f, R_f) are, respectively, the weight matrices (state, input command) of the finite horizon and the infinite horizon such that $Q = Q^T \geq 0,\ R = R^T \geq 0,\ Q_f = Q_f^T \geq 0$ and $R_f = R_f^T \geq 0$. The notation $\ell(.,.,.)$ and $\mathcal{P}_f(.,.)$ are, respectively, the stage cost and the terminal cost. It is important to note that the main motivation for introducing a terminal constraint set $\mathbb{X}_f(k)$ and a terminal cost function $\mathcal{P}_f(.,.)$ compared to a standard MPC scheme is to guarantee the stability of the closed-loop LTV system [20]. Suppose, then that the optimal control sequence $\hat{U}_k^* = \{\hat{u}_k^*(k), \dots, \hat{u}_k^*(k+N-1)\}$ that satisfies the control, state, and terminal constraints of (11b), has been determined. For each minimization of the cost function (11a), we apply only the first element $u(k, x(k)) = \hat{u}_k^*(k)$ of $\hat{U}_k^*$ that allows to have the solution $\Phi_k(k, \hat{x}_k^*, \hat{U}_k^*)$ for the system (9) at sample time k. Once the next state of the system is measured, the optimization problem is solved again, and the whole control procedure is repeated [20], [21]. In the following, we assume the persistent feasibility of the MPC law for any reference set $\mathbb{X}_f(k)$ and focus on the stability conditions. To investigate the uniform asymptotic stability of the tracking error, let introduce the following proposition :

Proposition 1 (Total optimal cost decrease): Wwe recall that $x(k)$ and U_k^* are bounded because of the sets $\mathbb{X}(k)$ and $\mathbb{U}(k)$ are closed and compact respectively, and we also know that $\|A(k)\| \leq \Theta_A$ and B are bounded. Therefore, $\mathcal{V}_N^*(k, x(k))$ is bounded and a decreasing function $\forall x \in \mathbb{X}$ and it is always feasible.

Proposition 2 ($\ell(\hat{x}_{k+N-1}^*, \hat{u}_{k+N-1}^*)$ is less than the terminal cost): Consider $\forall x \in \mathbb{X}_f(k) = \Omega_{ref}(k)$, and the function $\Delta\mathcal{V}_N^*(k, \hat{x}(k)) = \mathcal{V}_N^*(k-1, \hat{x}(k-1)) - \mathcal{V}_N^*(k, \hat{x}(k))$ is a locally positive definite function, if the following inequality holds $\ell(\hat{x}_{k+N-1}^*, \hat{u}_{k+N-1}^*) \leq \ell(\hat{x}_{k-1}^*, \hat{u}_{k-1}^*) - \Gamma(\hat{x}_k, \hat{x}_{k-1})$
in which $\Gamma(\hat{x}_k, \hat{x}_{k-1}) = \sum_{i=0}^{N-2} \|Q(\hat{x}_k^*(k+i) - \hat{x}_{k-1}^*(k+i)\|_2$, where $\hat{x}_k^*(k+i)$ is the solution of (11a-11b) at a sample time k when the control sequence $[u_{k-1}^*(k), \dots, u_{k-1}^*(k+N-2)]$ is applied.
Proof Consider the difference function value of the total optimal cos function at a sample time k given by $\Delta\mathcal{V}_N^*(k, \hat{x}(k)) = \mathcal{V}_N^*(k-1, \hat{x}(k-1)) - \mathcal{V}_N^*(k, \hat{x}(k)) \geq 0$. Therefore,

$$\begin{aligned} \Delta\mathcal{V}_N^* = & \sum_{i=0}^{N-1} \|Q\hat{x}_{k-1}^*(k+i-1)\|_2 + \sum_{i=0}^{N-1} \|R\hat{u}_{k-1}^*(k+i-1)\|_2 \\ & + \|P_f \hat{x}_{k-1}^*(k+N-1)\|_2 - \sum_{i=0}^{N-1} \|Q\hat{x}_k^*(k+i)\|_2 \\ & - \sum_{i=1}^{N-1} \|R\hat{u}_{k-1}^*(k+i-1)\|_2 - \|R\hat{u}_k^*(k+N-1)\|_2 \\ & - \|P_f \hat{x}_k^*(k+N)\|_2 \end{aligned} \tag{12}$$

Let $\hat{U}_{k-1}^* = [\hat{u}_{k-1}^*(k-1), \hat{u}_{k-1}^*(k), \dots, \hat{u}_{k-1}^*(k+N-2)]$ be the solution of the problem (11a-11b) at sample time $k-1$. Then for the sample time k, we have the following control sequence solution

$$\hat{U}_k^* = [\hat{u}_{k-1}^*(k), \dots, \hat{u}_{k-1}^*(k+N-2), \hat{u}_k^*(k+N-1)].$$

After simplification, the function $\Delta\mathcal{V}_N^*$ becomes

$$\begin{aligned} \Delta\mathcal{V}_N^* = & \underbrace{- \sum_{i=0}^{N-2} (\|Q\hat{x}_{k-1}^*(k+i)\|_2 + \|Q\hat{x}_k^*(k+i)\|_2)}_{\Gamma(\hat{x}_k, \hat{x}_{k-1})} \\ & + \underbrace{\|Q\hat{x}_{k-1}^*(k-1)\|_2 + \|R\hat{u}_{k-1}^*(k-1)\|_2}_{\ell(\hat{x}_{k-1}^*(k-1), \hat{u}_{k-1}^*(k-1))} \\ & - \underbrace{\|Q\hat{x}_k^*(k+N-1)\|_2 + \|R\hat{u}_k^*(k+N-1)\|_2}_{\ell(\hat{x}_k^*(k+N-1), \hat{u}_{k-1}^*(k+N-1))} \end{aligned} \tag{13}$$

By using the triangle inequality theorem $\|a\| - \|b\| \leq \|a-b\|$ on the first term of the relationship (13), we obtain the following inequality

$$\begin{aligned}\Delta\mathcal{V}_N^*(k,\hat{x}(k) \geq &- \Gamma(\hat{x}_k, \hat{x}_{k-1}) + \ell(\hat{x}_{k-1}^*, \hat{u}_{k-1}^*) \\ &- \ell(\hat{x}_{k+N-1}^*, \hat{u}_{k+N-1}^*)\end{aligned} \tag{14}$$

Since the value function $\Delta\mathcal{V}_N^*(k,\hat{x}(k) \geq 0$, then the condition of the proposition 2 is satisfied.

C. Haptic control Design based on the LTV-MPC Controller

To implement the LTV-MPC control algorithm, we consider the MWC-ergometer roller model of the simulator presented in Section II.A

$$\begin{cases} \Omega_i(k+1) = \frac{\Theta_1(k)}{\mathcal{I}_i}\Omega_i(k) + \frac{1}{\mathcal{I}_i}\tau_i(k) + \mathcal{W}(k) \\ \mathcal{W}(k) = \frac{1}{\mathcal{I}_i}(\Theta_2(k) + \tau_h(k)) \\ y(k) = \Omega_i(k) \end{cases} \tag{15}$$

Where the variable to be optimized is the ergometer motor torque $u(k) = \tau_i(k)$, the variable $y(k) = \Omega_i(k)$ denotes the output of the MWC simulator which is the MWC wheel speed, and $\mathcal{W}(k)$ is a known disturbance (see Section III.A). According to the algorithm defined in (11a)), the optimization problem to be solved is described as follows:

$$\begin{aligned}\mathcal{V}(\Omega(k)) = \min_{U_k}\Bigg\{&\sum_{i=0}^{N}\|Q(\Omega_k(k+i) - \Omega_{Ref_k}(k+i))\|_2 \\ &+ \sum_{i=0}^{N-1}\|R\ u_k(k+i)\|_2\Bigg\}\end{aligned} \tag{16a}$$

$$\begin{aligned} &s.t. \\ &\Omega(i+1) = A_k(\Theta_k)\Omega_k(i) + Bu_k(i) + \mathcal{W}_k(i), \quad {\scriptstyle i=k,\ldots,N-1} \\ &\tau_{min} \leq u_k(i) \leq \tau_{max}, \quad {\scriptstyle i=k,\ldots,k+N-1} \\ &\Omega_{min} \leq \Omega_k(i) \leq \Omega_{max}, \quad {\scriptstyle i=k,\ldots,k+N} \\ &\Omega_k(k) = \Omega(k) \end{aligned} \tag{16b}$$

$$\begin{aligned}\|Q(\Omega_k^*(k+N-1) - \Omega_{Ref_k}^*(k+N-1))\|_2 \\ + \|Ru_k^*(k+N-1)\|_2 \leq \epsilon\end{aligned} \tag{16c}$$

It should be noted that the constraint (16c) is the stability condition, such that ϵ is defined from the preposition (2), [20]. Once the optimization problem (16b is solved, the optimal control sequence $U^*(k) = [u_k^*(k), \ldots, u_k^*(k+N-1)]$ that satisfies the control, state, and terminal constraints is determined and only the first element $u(k,\hat{x}(k)) = u_k^*(k)$ of U_k^* is applied to compute the optimal simulator speed.

IV. Experimental results & Discussion

In this section, the evaluation and validation of the PSCHITT-PMR simulator are presented. Different standardized configurations of locomotion situations are defined and implemented in the virtual environment. The experimental results of the LTV-MPC controller are presented and compared with the results obtained with the controller approach developed in [13].

A. Validation of the LTV Model Online identification

In order to validate the LTV model of the MWC-Ergometer dynamics, we first set up a series of experimental tests that are carried out with a population weight ranging from $40kg$ to $80kg$. An excitation torque signal with an amplitude varying between $[-5, 5]$ is used to excite the dynamics of the ergometer in interaction with the MWC (7) in the entire region of the input and state constraints. To identify the dynamics of the MWC-Ergometer system, an online identification algorithm is implemented. The results of the experimental validation of the speed profile of the LTV model compared to that measured from the simulator are represented in Fig. (4). It should be noted that

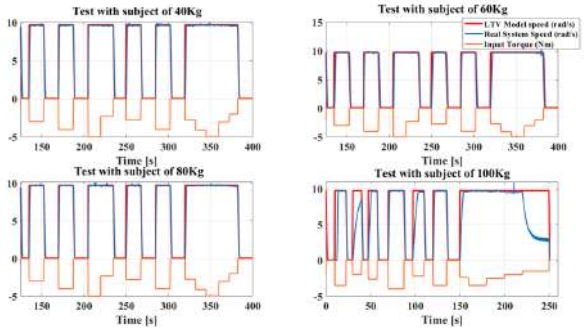

Fig. 4. Experimental results of the simulator LTV model (red curve) versus the simulator output (blue curve), in response to the excitation signal (orange curve).

Fig. 5. A-Real-life scenario. B-Simulated scenario.

the effect of the mass variation between $40-80Kg$ on the LTV model is very little visible with RMSE between 0.080 and 0.087. However, for a user weight greater than $100kg$ with a low propelling torque, the accuracy of the model begins to deteriorate, which represents the validity limit of the LTV model.

B. Validation of the Haptic Control Interface

Two types of wheelchair locomotion scenarios commonly encountered by users in urban environments are chosen to evaluate the haptic interface. The first type consists of reproducing wheelchair locomotion for a straight line, a slope/cross-slope and a turn.

(a) Starts in a straight line on a flat ground and turns with a variable radius of curvature, then returns to the initial position.
(b) Straight start on flat ground, start on a 4% slope with a rest after the slope, straight start, followed by a second 5% slope, rest after the slope, turn and descend the 5% slope.
(c) Start in a straight line on flat ground, go down a 7% cross slope, and maintain the path of the cross slope.

The second scenario consists of combining all the previous maneuvers to simulate, for example, an access and an exit of a building. To demonstrate the performance validity of the LTV-MPC haptic controller, the following parameters are considered: $A(k) \in [0.1175, 4.81]$, $K = -14.4$ and $\Theta_2 \in [-1.9666, 1.5336]$, $\|\mathbb{X}_k\| \leq 9.97[rad.s^{-}1]$ and $\|\mathbb{U}_k\| \leq 5[Nm]$. It should also be noted that the controller is implemented on SIMULINK in real-time and the optimization problem has been solved using the YALMIP environment with a calculation time of 4 ms. Fig. 6, illustrates the experimental results of scenario (a), in which the top figures show the trajectory carried out by the user. While the bottom figures show the reference tracking. Indeed, if the user performs scenario (a) on a real ground, when the radius of curvature is small enough, the user applies an opposite direction torque on each wheel (green rectangle) in order to turn. whereas when the radius of curvature is large enough, the user applies the same direction torque on both wheels. This behavior is

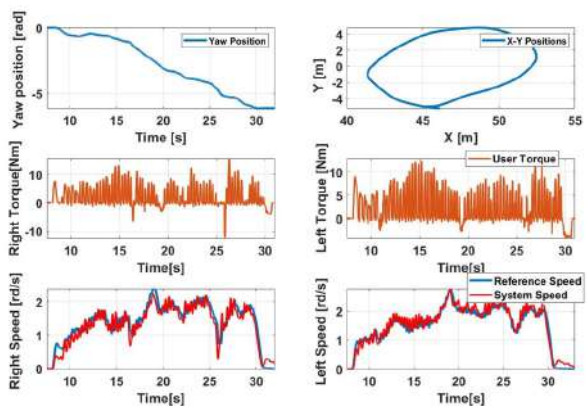

Fig. 6. Experimental validation of the haptic interface for the straight and turn scenario (a).

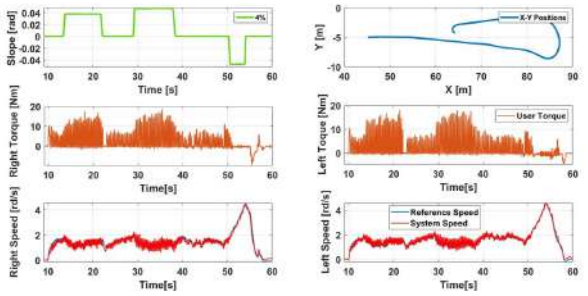

Fig. 7. Experimental validation of the haptic interface for the locomotion scenario for $2-4\%$ slopes (b).

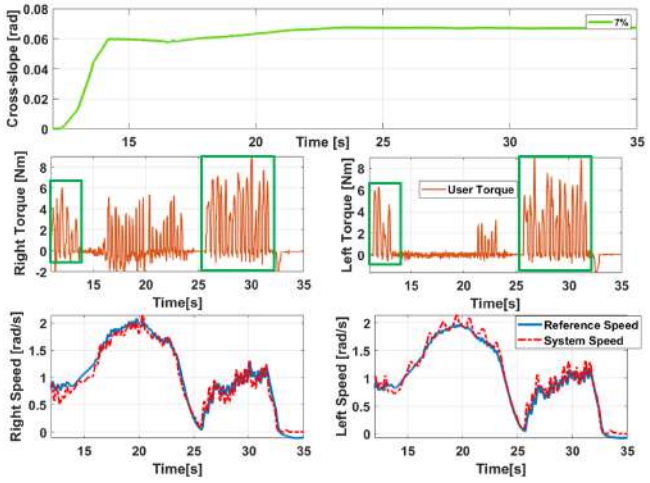

Fig. 8. Experimental validation of the haptic interface for the locomotion scenario for 7% cross slope (c).

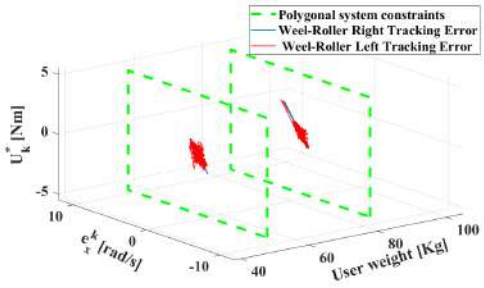

Fig. 9. Graphical evaluation of the LTV-MPC controller tracking error within the system constraint polygon.

similar to the one reproduced by the simulator. Regarding locomotion on a slope (scenario b), on a real terrain, it is observed that when the subject starts the slopes, he applies a higher propulsion torque of the same direction in order to compensate the gravitational force and maintain his instantaneous position. When the user goes down the slopes, he applies a torque opposite to the direction of the wheels to brake the movement, The same behavior is observed with the locomotion on the simulator, Fig. 7. Locomotion on a transverse slope is the most feared by people with reduced mobility. In fact, the direction of the wheelchair is perpendicular to the direction of the cross-slope. Therefore, the gravitational force is more important on one wheel than on the other, which obliges the user to compensate to maintain his current position. This same behavior is observed on the test of scenario (c) on the simulator for a transverse slope of 7%, where the position of the right wheel is on the high side of the slope compared to the position of the left wheel which is on the low side. It can be seen in Fig. 8 that the user applies a higher torque to the left wheel (green rectangle) than to the right wheel to maintain its trajectory on the cross slope.

C. Robustness with respect to uncertainties

To illustrate the effectiveness of the proposed controller, the experimental results of scenarios (d) and (e) are performed and compared to the results obtained with the EMPC controller proposed in [12]. The evaluation of the two controllers is done using three performance indices, root mean square error (RMSE), normalized root mean square error (NRMSE), and the correlation coefficient (R-value) presented in Tab. III.

$$RMSE = \sqrt{\frac{1}{N_{data}} \sum_{i=1}^{N_{data}} (x_i - x_{reel_i})^2}, \quad NRMSE = \frac{RMSE}{\overline{x}_{reel}}$$
$$R = \frac{\sum_{i=1}^{N_{data}} [(x_i - \overline{x})(x_{reel_i} - \overline{x}_{reel})]}{\sqrt{\sum_{i=1}^{N_{data}} (x_i - \overline{x}))^2 \sum_{i=1}^{N_{data}} (x_{reel_i} - \overline{x}_{reel})^2}} \tag{17}$$

Here, x_{reel_i} and N_{data} represent the measured output speed of the MWC simulator and the total number of data (estimated speed and actual speed), respectively. The experimental results are presented in Tab. III, where we notice that the performance indicators of the two approaches are very close in terms of value. However, the LTV-MPC approach is based on a simple model and adaptive to the variation and nonlinearity of the contact friction even during sudden variation of the reference speed when descending a slope, which makes the LTV-MPC approach more promising in the context of this work. Lastly, Figure 9 shows a graphical presentation of the LTV-MPC controller tracking error within the system constraint polygon. These results clearly confirm that the LTV-MPC approach stabilizes the tracking error around the origin even with different weights during the sudden variation of the reference speed with a braking torque disturbance.

V. Conclusion

In this work, a wheelchair locomotion simulation platform driven by a haptic interface has been presented. Based on a dynamic 3D model of the wheelchair, the designed haptic interface allows us to

TABLE III
PERFORMANCE EVALUATION OF EACH CONTROLLER USING THE STATISTICAL INDICATORS RMSE, NRMSE, R-VALUE.

			LTV-MPC				EMPC		
Subject	Gender/Age	Weights (Kg)	Side	RMSE	NRMSE	R Value	RMSE	NRMSE	R Value
S_1	M-40 yo	85	Left	0.3604	0.0730	0.9667	0.2571	0.0382	0.9897
			Right	0.3640	0.0583	0.9653	0.2245	0.0288	0.9919
S_2	F-28 yo	53	Left	0.2925	0.0786	0.9658	0.1953	0.0388	0.9873
			Right	0.2588	0.0713	0.9720	0.1817	0.0358	0.9890

simulate a wide range of environmental situations that people with reduced mobility face in their daily lives. Furthermore, this paper gives particular attention to the design and implementation of the LTV-MPC-based haptic controller using a linear model with time-varying parameters. The LTV-MPC controller is designed taking into account the input and output constraints of the real system, the variation of the contact friction between the wheels of the wheelchair and the roller bench due to the different weights of the users (between 40 and $100kg$), and the internal and external disturbances i.e., the torque of the user during the pushing phase. A complete stability analysis of the LTV-MPC controller was presented by introducing sufficient conditions for uniform asymptotic convergence of the tracking error of the closed-loop system at the origin. Realistic and standardized experimental scenarios were defined in order to validate and evaluate the performance of the controller by comparing it to an EMPC scheme based on a nonlinear model. The experimental results showed that the LTV-MPC controller is as able to follow the reference speed and ensure the durability of stability over time as the EMPC controller even during difficult driving maneuvers such as hill climb, turns and hill descent, which clearly confirms that the LTV-MPC approach stabilizes the tracking error in the vicinity of the origin even with different weights, during the sudden variation of the reference speed with a braking torque disturbance. For future work, the proposed haptic interface will be validated by an experimental campaign in the framework of the CapaCITIES project, involving a dozen subjects with motor disabilities.

REFERENCES

[1] J. W. Chow, and C. E. Levy. "Wheelchair propulsion biomechanics and wheelers' quality of life: an exploratory review." Disability and Rehabilitation: Assistive Technology 6.5 (2011): 365-377.

[2] C. Sauret, et al. "Assessment of field rolling resistance of manual wheelchairs." Journal of Rehabilitation Research and Development 49.1 (2012): 63-74.

[3] Kwarciak, Andrew M., et al. "Comparing handrim biomechanics for treadmill and overground wheelchair propulsion." Spinal cord 49.3 (2011): 457-462.

[4] De Klerk, Rick, et al. "Measuring handrim wheelchair propulsion in the lab: a critical analysis of stationary ergometers." IEEE Reviews in Biomedical Engineering 13 (2019): 199-211.

[5] R. Aissaoui, and D. Gagnon. "Effect of Haptic Training During Manual Wheelchair Propulsion on Shoulder Joint Reaction Moments." Frontiers in Rehabilitation Sciences (2022): 43.

[6] Colin S. Harrison, Mike Grant, Bernard A. Conway; Haptic Interfaces for Wheelchair Navigation in the Built Environment. Presence: Teleoperators and Virtual Environments 2004; 13 (5): 520–534. doi: https://doi.org/10.1162/1054746042545265

[7] Chénier, Félix, et al. "Unmatched speed perceptions between overground and treadmill manual wheelchair propulsion in long-term manual wheelchair users." Gait and posture 61 (2018): 398-402.

[8] K. Ly, P. Karg, J. Kreimeier, and T. Götzelmann. 2022. Development and Evaluation of a Low-cost Wheelchair Simulator for the Haptic Rendering of Virtual Road Conditions. In Proceedings of the 15th International Conference on PErvasive Technologies Related to Assistive Environments (PETRA '22). Association for Computing Machinery, New York, NY, USA, 32–39. https://doi.org/10.1145/3529190.3529195

[9] C. Brown, and John McPhee. "Predictive forward dynamic simulation of manual wheelchair propulsion on a rolling dynamometer." Journal of biomechanical engineering 142.7 (2020): 071008.

[10] R. De Klerk, et al. "a novel servo-driven dual-roller handrim wheelchair ergometer." IEEE Transactions on Neural Systems and Rehabilitation Engineering 28.4 (2020): 953-960.

[11] F. Chénier, P. Bigras, and Ra. Aissaoui. "A new wheelchair ergometer designed as an admittance-controlled haptic robot." IEEE/ASME Transactions on Mechatronics 19.1 (2013): 321-328.

[12] L. R Crichlow, et al. "A full motion manual wheelchair simulator for rehabilitation research." Proceedings of the 2011 annual RESNA conference. 2011.

[13] T. Bentaleb, et al. "A real-time multi-objective predictive control strategy for wheelchair ergometer platform." 2019 IEEE International Conference on Systems, Man and Cybernetics (SMC). IEEE, 2019.

[14] A. Ait-Ghezala, C. Sentouh, and P. Pudlo. "Direct Model-Reference Adaptive Control for Wheelchair Simulator Control via a Haptic Interface." IFAC-PapersOnLine 55.29 (2022): 49-54.

[15] V.T. Nguyen, et al. "On a complete dynamical model of manual wheelchair for virtual reality simulation platform." 2019 IEEE International Conference on Systems, Man and Cybernetics (SMC). IEEE, 2019.

[16] L. C. A. Silva, F. C. Corrêa, J. J. Eckert, F. M. Santiciolli & F. G. Dedini. (2017). A lateral dynamics of a wheelchair: identification and analysis of tire parameters, Computer Methods in Biomechanics and Biomedical Engineering, 20:3, 332-341, DOI: 10.1080/10255842.2016.1233327

[17] F. O. Medola, P. V. Dao, J. J. Caspall and S. Sprigle, "Partitioning Kinetic Energy During Freewheeling Wheelchair Maneuvers," in IEEE Transactions on Neural Systems and Rehabilitation Engineering, vol. 22, no. 2, pp. 326-333, March 2014, doi: 10.1109/TNSRE.2013.2289378.

[18] J. Na, Q. Chen, & X. Ren. Chapter 1 - Friction Dynamics and Modeling. In Emerging Methodologies and Applications in Modelling, Adaptive Identification and Control of Uncertain Systems with Non-smooth Dynamics, 2018, Pages 11-18, ISBN 9780128136836, https://doi.org/10.1016/B978-0-12-813683-6.00003-9.

[19] A. Brosch, S. Hanke, O. Wallscheid and J. Böcker, "Data-Driven Recursive Least Squares Estimation for Model Predictive Current Control of Permanent Magnet Synchronous Motors," in IEEE Transactions on Power Electronics, vol. 36, no. 2, pp. 2179-2190, Feb. 2021, doi: 10.1109/TPEL.2020.3006779.

[20] P. Falcone, F. Borrelli,H.E. Tseng, J. Asgari and D. Hrovat, (2008), Linear time-varying model predictive control and its application to active steering systems: Stability analysis and experimental validation. Int. J. Robust Nonlinear Control, 18: 862-875. https://doi.org/10.1002/rnc.1245

[21] F. Borrelli, A. Bemporad, and M. Morari. (2017). Predictive Control for Linear and Hybrid Systems. Cambridge: Cambridge University Press. doi:10.1017/9781139061759

[22] A. Bemporad, et al. "The explicit linear quadratic regulator for constrained systems." Automatica 38.1 (2002): 3-20.

[23] G. De Nicolao, L. Magni, and R. Scattolini. "Stabilizing receding-horizon control of nonlinear time-varying systems." IEEE Transactions on Automatic Control 43.7 (1998): 1030-1036.